Progress In Electromagnetics Research M, Vol. 69, 23–36, 2018

Would the Human Brain Be Able to Erect Specific Effects due to the Magnetic Field Component of an UHF Field via Magnetite Nanoparticles?

Simona Miclaus[1, *], Cora Iftode[2], and Antoniu Miclaus[3]

Abstract—In 2016 a study reported observing a concentration of magnetite nanocrystals in human brains, with four orders of magnitude larger than previously thought. In the context of magnetite's role and function inside the human brain not being properly understood, this development prompts a question concerning the impact that a significant magnetic near-field component, in the hundreds of MHz range, might have on power loss in tissues having ferrimagnetic properties. This article highlights the importance of thorough research on possible thermal and non-thermal effects that could be caused by the magnetic field component to which one could be exposed while using certain communication devices near or in front of the head. Furthermore, this article provides preliminary estimations of magnetic contribution to the specific absorption rate (SAR) of energy deposition in tissues, using two approaches — one based on existing research concerning magnetic hyperthermia, and the other one based on a simulation model that takes into account the magnetic properties of tissues. By simulating the propagation of a 440 MHz wave in a "magnetic" (as opposed to pure dielectric) brain, we observed changes of the SAR values, and, more importantly, superficial hot spots appeared at the surface of small magnetite particles, distributed in the homogenous brain.

1. INTRODUCTION

The currently available literature concerning effects of using radiofrequency (RF) communication devices emitting in the very high frequency (VHF) or ultrahigh frequency (UHF) bands in the proximity of the head (brain, eyes) deals exclusively with one biological effect, the thermal one, which is due to the dielectric heating of tissues [1]. The dielectric heating is caused by the electric field strength (E) component of radio waves propagating through dielectric materials that have complex electrical permittivity; the energy release is quantified by the energy specific absorption rate (SAR), which — when caused by the E-field component of the radio wave — we will denote as SAR_E. A lack of evidence that human tissue (brain tissue, specifically) contains a significant amount of magnetic material has led to the influence of the magnetic field strength (H) component of radio waves being mostly neglected by scientists, inasmuch as research pertaining to the safe near-the-head use of communication devices (mobile phones, walkietalkies, portable transceivers, etc.) was concerned — since no significant effects, thermal or otherwise, were expected to occur. The one notable exception is presented in [2], where it is proven that a correct RF energy absorption assessment in the near-field may be done by using also the magnetic component of RF fields.

It was recently discovered that the brain could contain as much as 0.2–12 µg of magnetite in 1 g of dry cerebral tissue; furthermore, this discovery demonstrates the existence of exogenic magnetite at

Received 8 March 2018, Accepted 9 May 2018, Scheduled 29 May 2018

* Corresponding author: Simona Miclaus (simo.miclaus@gmail.com).

[1] Technical Sciences Department, "Nicolae Balcescu" Land Forces Academy, 3-5 Revolutiei St., Sibiu 550170, Romania.

[2] Measurements and Optical Electronics Department, Politehnica University of Timisoara, 2 Vasile Parvan St., Timisoara 300223, Romania. [3] Faculty of Mathematics and Computer Science, Babes-Bolyai University, 1 Mihail Kogălniceanu St., Cluj-Napoca 400084, Romania.

the cerebral level, arising from air pollution [3] — in addition to the previously discovered biogenic magnetite, originally observed in 1992 by Kirschvink et al., in trace amounts [4]. These quantities are roughly 4 orders of magnitude higher than the previous estimations.

Magnetite has a high affinity for absorbing the H-field component of radio waves at frequencies in the UHF range [5]. Therefore, the existence of significant amounts of magnetite nanocrystals located in human brain tissue needs to be carefully investigated as a potential health risk factor, taking into account both potential thermal and non-thermal effects, particularly since magnetite nanocrystals' interaction with the neurosensory system (via breaking of biochemical bonds) could not be excluded [6, 7]. Furthermore, direct cellular effects have also been reported, both in the presence and in the lack of a perceptible macroscopic temperature rise [8].

While the biological impact of VHF and UHF ranges was largely ignored in studies concerning the biological impact of H-field on magnetite nanocrystals naturally present in tissues. Low frequency (LF) and medium frequency (MF) ranges have been researched intensively over a few decades, due to the applications of magnetic fluid hyperthermia in bio-medical topics. Magnetoreception is studied, and [9] investigates either the influence of a static H-field on biological sensing or the collateral effects of extremely low frequencies (of the order of a few Hertz). Additionally, intensive research is conducted on the potential of tiny artificially synthesized magnetite crystals for destroying carcinoma via local temperature increase; these crystals, forming ferrofluids, are injected in tissues and exposed to H-fields in the 100–300 kHz frequency range [10], this direction of research providing a good starting point for assessing the effects of the VHF and UHF frequency bands.

The biogenic magnetite nanocrystals found in the human brain have several relevant properties [3, 6, 11–14]: euhedral geometry (cuboctahedral or prismatic) manifesting crystallographic perfection; chemical purity; they can be encountered as either superparamagnetic (SPM) single-domain (SD) crystals — the most common or multi-domain (MD); the transition from the SPM phase to the SD one typically occurs at particle sizes of about 25–30 nm, while the SD to MD transition happens at sizes of about 70 nm. The large magnetic momentum of the SD nanocrystals makes it possible that they might affect biological processes — either through the H-field they generate or under the influence of an external H-field [12]. The crystals are intracellular, and occasionally they form chains, are bound to the cell membrane, and have a saturation magnetization $M_s = 4.5 \times 10^5$ A/m; occasionally, the crystals show unusual morphology [4]. The weight ratio between biogenic magnetite and the total crystals amounts in the brain is estimated at 1 : 500 [13]. The biogenic magnetite crystals in the human brain tend to display a rounded/spherical geometry and to have dimensions in the 5–35 nm range (median diameter in the 14–10 nm range), with a mean circularity of 0.92. The exogenic crystal typically falls in the 10–150 nm range, with some observed crystals exceeding 200 nm [3]. The magnetite distribution over the entire human brain's volume is uniform, except the meninges [4]; the average concentration of magnetite in the brain tissue is 4 ng/g, whereas in the meninges it averages 70 ng/g [4]. The 2016 findings of the Maher group [3] indicate a maximum total concentration of magnetite (biogenic plus exogenic) per wet cerebral tissue of 160 µg/g; this is a four orders of magnitude increase in ferrimagnetic content in the brain, compared to the values estimated in the '90s (pollution being the primary suspected cause). This begs a question concerning the contemporary risks caused to human health by the usage of equipment operating in the VHF and UHF bands, in close proximity to the head or, indeed, any other organ with significant magnetic content.

Published research into this topic is scarce; yet a few studies exist, which suggest a possible link between H-field strength and the response of biological material that has magnetic content; for example, the authors of [15] previously reported that a 0.25–2 MHz H-field had affected the iron cage proteins called ferritins, and their functioning through a mechanism that was neither thermal nor caused by the E-field component of the radio wave — rather, it consisted in the reduction of the rate of iron intake/release after the protein was exposed to the RF field; this study further concludes that the effect depends on the product between the H-field's frequency and amplitude, as well as on the relative concentrations of ferritin and iron chelator. This is likely the first report of 1 MHz low strength field acting non-thermally at the molecular level, and modifying processes in which ferromagnetic nanoparticles were involved. A later study [7] concluded that it was necessary that this effect was taken into consideration when assessing the biological effects of environmental RF fields.

Investigations into the functioning of the brain also provided related conclusions: the authors of [16]

hypothesized that the ability to respond to low-intensity H-fields could be a form of sensory transduction quantified by evoked potentials. By applying an H-field with a flux density of 200 μT at 60 Hz and analyzing the electroencephalograms (EEG) using nonlinear methods, the group concluded that the application and the removal of the H-field appeared as sensorial stimuli do. The same group later tested even smaller magnetic flux densities (1 μT and 5 μT) at 60 Hz, and by analyzing the electrical activity of the brain once more, concluded that the fields were detected and reacted to as ordinary somatic stressors would [17].

Researchers of [18] studied the effect of radio waves on the EEG rhythms of humans, using a 13 cm quarter-wave antenna placed 10 cm away from the head, to emit a pulse-modulated signal over a carrier frequency of 450 MHz (thus simulating a portable radio communication transceiver). The experiment resulted in some of the EEG rhythms being significantly altered in response to the frequency modulation of the UHF signal, while the experiment only considered the incident E-field strength (with a power density of 0.16 mW/cm^2), neither measuring nor considering the H-field component. It is noteworthy that the authors reported that the EEG changes "were more obvious at the beginning of the exposure segments" — a conclusion shared with the unrelated study of the H-field's impact on ferritins and their functioning [7]. Hinrikus' group followed up with experiments using two field levels, quantified by determining the SAR based on E-field strength, applying $\mathrm{SAR}_{E1} = 0.303$ W/kg and $\mathrm{SAR}_{E2} = 0.003$ W/kg to the brain of human volunteers [19]. The results were positive once more, and the influence of the field was present in different proportions. The researchers reported that "decreasing the SAR 100 times reduced the related changes in the EEG three to six times and the number of affected subjects, but did not exclude the effect." While still no assessment of the H-field component was done and no connection drawn between it and the observed effects, the authors were able to highlight a (clearly non-thermal) effect even when SAR_E was so low that it reached the limit of detection. A later output of Hinrikus' group, published in 2017, attempted to explain the effect purely from the dielectric response perspective [20]. However, antennas similar to the one used by Hinrikus' group have a near-field distribution (10 cm from the antenna, at 450 MHz) in which the H-field component is more significant than the E-field component, with respect to their magnitudes relative to the limits provided in the human safety standards [21]. This fact begs the question: how does the H-field contribute to the reported effects observed at 450 MHz?

Other research exists, which relates to the question hereby asked. One study reports that similar changes in brain's physiology occurred, both caused by a 2 Hz pulse-modulated RF field (900 MHz carrier frequency) and caused by a 2 Hz pulsed magnetic field, showing that the effects observed on EEGs were not specific to the pulse-modulated field [22]. Also, studies concerning the blood-brain-barrier (BBB) permeability show that moderate heat dissipated by nanocrystals of magnetite under the effect of a RF field could increase the permeability of the BBB by transiently and locally opening it [23], and that non-thermal levels of SAR_E at hundreds of MHz also increase BBB permeability [24, 25].

The cited research clearly indicates that investigations into the possible effects caused by UHF emitting devices on tissues with ferro- or ferrimagnetic content are at the very least worthwhile, if not necessary; this is so, particularly when one considers that UHF band equipment is permanently used in everyday life, as well as medical investigations and treatments. This paper attempts to contribute by providing a preliminary estimation of the order of magnitude with which H-field component of the near-field contributes to the total rate of energy deposition in such tissues.

2. MATERIALS AND METHODS

The purpose of our investigations is to assess how large the specific rate of magnetic energy deposition, SAR_H, might be in a "magnetic brain", assuming that the incident wave penetrates the scalp. Since it would be impractical to consider doing meaningful experiments on actual human brains, the necessary investigations are performed using modeling. Specifically, two approaches are taken: a) microscopic dosimetry: SAR_H is assessed using available models of magnetic hyperthermia of nanoparticles; and b) macroscopic dosimetry: a propagation of the radio wave in "dielectric" brain tissue is simulated, followed by a simulation of the same brain model, to which small magnetite particles are added — thus mimicking a "magnetic brain"; this approach leads to an assessment of the total SAR, at macroscopic level.

2.1. Microscopic Dosimetry for Loss Determination in Magnetite Nanoparticles

There are three distinct mechanisms that lead to heat generation when a magnetite nanocrystal is exposed to the H-field component of a radio wave: a) Neel relaxation, caused by the rotation of the magnetic moments, ignoring the rotation of the entire particle; b) Brownian relaxation, caused by the rotation of the entire particle in the alternative field; and c) hysteresis loss, caused by the shifting of magnetic domain walls in multi-domain materials; the later becomes significant in particles larger than a critical grain volume V_c, which, in case of magnetite exposed to 200 kHz, occurs at a diameter of about 15 nm [26]. All of these depend on the size, shape, crystalline anisotropy, morphology and the degree of aggregation/agglomeration of nanoparticles [26–34]. It should be noted that, in the general case, a fourth mechanism is possible as well — the generation of Foucault (eddy) currents, consisting in resistive heating caused by a rapidly varying magnetic flux. However, this is irrelevant for nanoparticles, since it only appears significant in bulk materials or at centimetric scale.

The Neel relaxation time, τ_N is given in [26]:

$$\tau_N = \frac{\tau_0}{2}\sqrt{\pi\frac{kT}{KV}}e^{\frac{KV}{kT}} \tag{1}$$

where τ_0 is the attempt time (in the 10^{-9}–10^{-11} s range), k the Boltzmann constant, T the absolute temperature, K the anisotropy constant (given by either crystalline or shape effects), and V the volume of the particle. The typical anisotropy values are $K = 40\,\mathrm{kJ/m^3}$ (high), $K = 25\,\mathrm{kJ/m^3}$ (average), and $K = 10\,\mathrm{kJ/m^3}$ (low). Magnetocrystalline anisotropy of bulk magnetite is in the 11–14 $\mathrm{kJ/m^3}$ range [26]; shape anisotropy is related to the nanoparticles' deviations from sphericity, such that, for instance, an aspect ratio of 1.4 yields an expected contribution of $20\,\mathrm{kJ/m^3}$ to the total K. The typical range for the magnetic anisotropy constants in magnetite nanoparticle ensembles is 10–41 $\mathrm{kJ/m^3}$.

The Brownian relaxation time, τ_B, is given by:

$$\tau_B = \frac{3\eta V_H}{kT} \tag{2}$$

where η is the dynamic viscosity of the medium, and V_H is the hydrodynamic volume of the particle, membrane included. For uniformly distributed nanoparticles in a medium, the effective relaxation time of a particle, τ_{eff}, is defined as:

$$\frac{1}{\tau_{eff}} = \frac{1}{\tau_N} + \frac{1}{\tau_B} \tag{3}$$

If H-field strength impinging magnetite crystals has a variation in time t of the form:

$$H(t) = \mathrm{Re}\left[H_0 e^{j\omega t}\right] = H_0\cos(\omega t) \tag{4}$$

then the complex susceptibility of magnetite will be:

$$\chi = \chi' + j\chi'' \tag{5}$$

where real part of susceptibility is:

$$\chi' = \frac{\chi_0}{1 + (\omega\tau_{eff})^2} \tag{6}$$

And imaginary part of susceptibility is:

$$\chi'' = \frac{\omega\tau_{eff}\chi_0}{1 + (\omega\tau_{eff})^2} \tag{7}$$

In the expressions above, ω is the field pulsation ($\omega = 2\pi f$), χ_0 is the equilibrium susceptibility (or at direct current-DC) being expressed as:

$$\chi_0 = \frac{\mu_0 M_s^2 V}{kT} \tag{8}$$

where M_s is the saturation magnetization, V the volume of the particle's magnetic core, and μ_0 the permeability of free space. For magnetite nanocrystals M_s takes values in the (30–60) $\mathrm{A\cdot m^2/kg}$ range [26].

The heat dissipation due to H field alone, will be composed of two terms (relaxation and hysteresis):

$$SAR_H = SAR_{H\_relax} + SAR_{H\_hyster} \tag{9}$$

The relaxation effect is expressed here by SAR_{H_relax}:

$$SAR_{H\_relax} = \pi\mu_0 f H_0^2 \chi'' \frac{1}{\rho} = \pi\mu_0 f H_0^2 \chi_0 \frac{\omega\tau_{eff}}{1+(\omega\tau_{eff})^2}\frac{1}{\rho} \tag{10}$$

where H is the magnitude of the magnetic field and ρ the particles' mean mass density. A change in anisotropy leads to large variations of SAR_{H_relax} for any given particle diameter; the most impacted term is τ_N, since the anisotropy energy KV is part of the argument to the exponential function therein. Therefore, an anisotropy change will lead to high variations of SAR_H for small particles, and SAR_{H_relax} reaches its maximum value when $\omega\tau_{eff}$ is 1; the same applies to the imaginary part of the susceptibility, χ'', with the corresponding frequency called the critical frequency f_c.

For field frequencies $f \ll f_c$ (or $\omega\tau_{eff} \ll 1$):

$$SAR_{H\_low} = 2\pi^2\mu_0 f^2 H_0^2 \chi_0 \frac{\tau_{eff}}{\rho} \tag{11}$$

depending on the square of both frequency and magnitude of the field.

For frequencies $f \gg f_c$ (or $\omega\tau_{eff} \gg 1$):

$$SAR_{H\_high} = \mu_0 H_0^2 \chi_0 \frac{1}{2\tau_{eff}\rho} \tag{12}$$

which does not depend on the frequency anymore.

From a calorimetric point of view, the specific absorption rate of magnetic energy deposition may be quantified by the formula:

$$SAR_H = \frac{cV_s}{m}\frac{dT}{dt} \tag{13}$$

where c is the sample's specific heat capacity, m the mass of magnetic particles, V_s the sample's volume, and dT/dt the temperature increment caused by the exposure. If a brain (br) is considered, containing magnetite (mag), a correction of its specific heat capacity is required [35]. When the correction factor is applied, we arrive at the effective value:

$$c_{eff} = \frac{(1-\phi)\,\rho_{br}c_{br} + \phi\rho_{mag}c_{mag}}{(1-\phi)\,\rho_{br} + \phi\rho_{mag}} \tag{14}$$

where $\rho_{\mathrm{br}} = 1100\,\mathrm{kg/m^3}$, $c_{br} = 3630\,\mathrm{J/kg\cdot K}$, $\rho_{\mathrm{mag}} = 5200\,\mathrm{kg/m^3}$, $c_{mag} = 937\,\mathrm{J/kg\cdot K}$ [26], and ϕ is the volume fraction of magnetite (both types) in the human brain which we computed based on data from [3] to be $\Phi = 3.4\times10^{-5}$. With these values, the effective specific heat of the brain becomes $c_{eff} = 3630.92\,\mathrm{J/kg\cdot K}$.

SAR_{H_hyster}, the hysteresis loss contribution to the total SAR_H, was previously analyzed at a frequency of 80 kHz [27]. The observed SAR_{H_hyster} of magnetite particles depended strongly on the particles' sizes: for diameters larger than 46 nm, it increased as the particle size decreased, the hysteresis loss becoming the main dissipation mechanism; for small SPM particles however (7.513) nm, hysteresis loss decreased to zero leaving just relaxation losses, themselves rather small at the experimental frequency of 80 kHz. However, somewhat contrary findings have been recently reported in the case of SPM particles' heating [36]: for crystals larger than approx. 100 nm a significant hysteresis loss occurs, due to the shifting of the particle's domain walls [37]. This conclusion also applies to small particles — which are SD, rather than SPM. The coercitivity field strength, H_{coerc}, is a function of the particle's volume V and is significant for volumes larger than a critical volume V_c [26]:

$$H_{coerc} = \frac{2K}{M_s}\left(1-\sqrt{\frac{V_c}{V}}\right) \tag{15}$$

The ratio between specific (volumic) magnetic power dissipation p_m and specific electric power dissipation p_e, at any frequency f, can be calculated by using the expression [38]:

$$\frac{p_m}{p_e} = \frac{\varepsilon_0}{\mu_0}\frac{\varepsilon''}{\mu''}\frac{E_0^2}{H_0^2} \tag{16}$$

This relation shows that provided that the excitation field components are both known and that the biological target is characterized both electrically and magnetically, it is rather simple to assess the ratio of either field component, in relation to the entire dissipation. This in turn points to the usefulness of precise measurements of both the electric permittivity and magnetic permeability, and while in the case of a magnetite-containing human brain, doing so would be impractical, and it is expected that a model could be constructed by studying magnetotactic bacteria suspensions which contain magnetosomes.

2.2. Macroscopic Dosimetry for Loss Calculations in a Homogeneous Model of Brain Not-Containing and Containing Small Magnetite Spheres

In order to highlight the potential impact of the presence of ferrimagnetic material on power loss in the brain tissue due to exposure, by comparing SAR values corresponding to a non-magnetic and a magnetic brain respectively, a simple homogeneous dielectric brain model was constructed; five small magnetite spheres have been inserted into it, to give it some magnetic properties. This brain model was placed in the near field of a modeled radiation source, constructed as a portable transceiver monopole antenna emitting a continuous wave at $f = 440\,\text{MHz}$. ANSYS HFSS software was used, which applies the finite element method solver for electromagnetic structures and simulating propagation; simulations were run with and without the magnetic material included.

The simulation approach was developed gradually, resulting in the first study which computes the total SAR in a tissue model — including both SAR_E and SAR_H. A very thin (2 mm) monopole antenna with a length of $L = 18\,\text{cm}$, connected to a $50 \times 90\,\text{cm}$ ground plane, was used as the source of exposure; this is similar to the real portable transceivers'. The excitation was provided by a voltage source such that the input power of the antenna was 1 W; the antenna efficiency calculation was computed as 92.6%, thus the radiated power was $P_{rad} = 0.93\,\text{W}$. In the near field of this antenna, at a distance of $D = 13\,\text{cm}$, the center of an ellipsoidal homogeneous brain model was placed; the minimal distance between the brain's surface and the antenna was 8 cm. Fig. 1 depicts the experimental configuration and the dimensions of the objects by using perspective view and projections. Inside the homogeneous brain, in the second considered case, five small magnetite spheres were inserted, placed as follows: spheres 1, 2 and 3 were placed in the same "vertical" plane at the same distance to the surface of the transceiver (where a "vertical" plane in the brain ellipsoid is one parallel to the transceiver surface and to the antenna); sphere 4 was placed the closest to the transceiver surface, while sphere 5 the most distant.

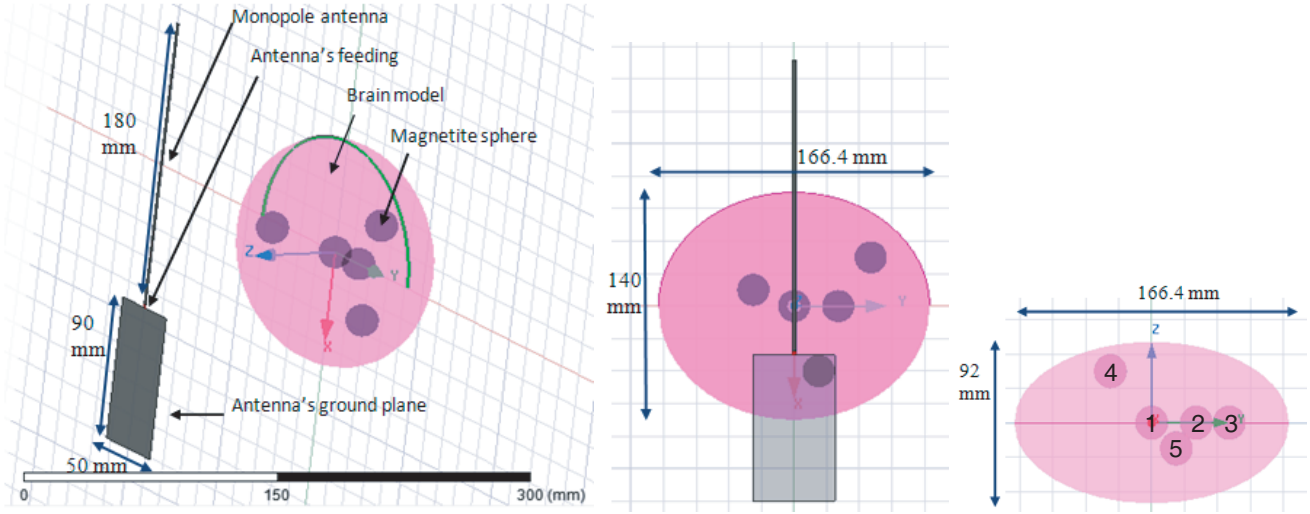

Figure 1. The exposure configuration: the dielectric ellipsoidal brain model (pink) in which five small magnetite spheres were placed, thus obtaining the "magnetic brain"; the brain is placed in front of a monopole antenna emitting at 440 MHz; (a) perspective view of configuration; (b) front view; (c) top view.

The volume of the ellipsoidal brain model was $V_{br} = 1129.7597\,\text{cm}^3$ while one magnetite sphere had the radius $r_{sf} = 1\,\text{cm}$ (volume $V_{sf} = 4.186\,\text{cm}^3$). The mass density of the brain tissue was considered to be $1100\,\text{kg/m}^3$, while for magnetite $5200\,\text{kg/m}^3$ it was used. The volumic fraction of magnetic material in the brain was therefore derived to be $\Phi = 0.0185$ — which is 540 times larger than the one reported in real brains by [3]. Determination of the total SAR ($\text{SAR}_E + \text{SAR}_H$) was made indirectly, by using the software computed mean volume loss density (MVLD), in two situations: a) non-magnetic brain (purely dielectric — without including the magnetite spheres); b) magnetic brain (brain with the spheres included). MVLD provided the electric and magnetic losses separately, and on its basis, the mean SAR_E and SAR_H values were calculated (volumes and masses being known); the material properties of the brain and magnetite at 440 MHz used for the simulations are presented in Table 1.

Table 1. Electric and magnetic properties of brain tissue and magnetite.

Electric/magnetic properties	Brain tissue (pure dielectric)	Magnetite
Relative permittivity	$\varepsilon'_r = 43.48$	$\varepsilon_r = 50$
Conductivity	$\sigma = 0.87\,\text{S/m}$	$\sigma = 3\,\text{S/m}$
Dielectric loss tangent	$\delta_e = 0.49$	$\delta_e = 2.5$
Relative permeability	$\mu'_r = 1$	$\mu'_r = 1.9$
Magnetic loss tangent	$\delta_m = 0$	$\delta_m = 0.3$

3. RESULTS AND DISCUSSION

3.1. Microscopic Dosimetry Approach

The first considered case was that of magnetite nanoparticles dispersed in water, with radii in the 5–15 nm range, and the following properties: very small anisotropy constant $K = 6\,\text{kJ/m}^3$; temperature $T = 297\,\text{K}$; medium viscosity $\eta = 8.9 \cdot 10^{-4}\,\text{Pa}\cdot\text{s}$ (water's); $\tau_0 = 10^{-10}\,\text{s}$; mass density $\rho = 5200\,\text{kg/m}^3$; hydrodynamic volume as particle's volume V enlarged by a 5 nm-wide layer; saturation magnetization $M_s = 60\,\text{A}\cdot\text{m}^2/\text{kg}$. The results of relaxation times variation as a function of particle dimension are presented in Fig. 2. The effective relaxation time varies between $10^{-10}\,\text{s}$ and $10^{-5}\,\text{s}$, depending on the particle radius. For the frequency of interest, $f = 440\,\text{MHz}$, the radius of particles, which would be heated the most, is 6.5 nm; in this particular case we calculated that $\chi_0 = 9.71 \cdot 10^{-5}$, and considering

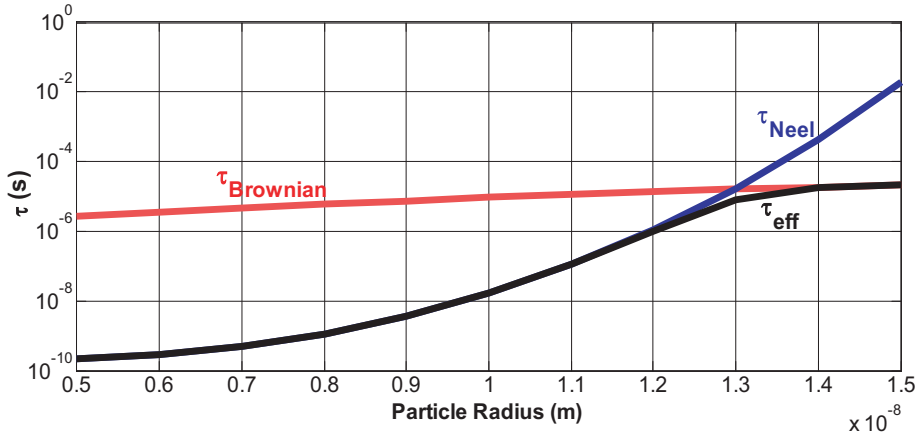

Figure 2. Relaxation times of magnetite nanocrystals owing very reduced anisotropy in function of their radius.

an amplitude $H = 0.35\,\mathrm{A/m}$, the maximum SAR_H (based exclusively on relaxations, for $\omega\tau_{eff} = 1$) is:

$$SAR_{H\_\max} = \frac{1}{2}\pi\mu_0 f H_0^2 \chi_0 \frac{1}{\rho} \approx 2 \times 10^{-6}\,\mathrm{W/kg} \tag{17}$$

It should be noted that SAR_{H_hyster} was completely neglected. Particles with diameters larger than 13 nm will have lower SAR_H values, thus they will not depend on the frequency of the field, but only on the H-field strength: $\mathrm{SAR}_{H\_high} = \mu_0 H_0^2 \chi_0 \frac{1}{2\tau_{eff}\rho}$. It can be then expected that, for large nanoparticles (tens of nm), the relaxation contribution to the heating would be at least of the order of $\mathrm{SAR}_{H\_high} = 10^{-7}$–$10^{-8}\,\mathrm{W/kg}$. Fig. 3 shows a decrease in the real part of susceptibility as frequency increases, as well as the fact that the imaginary part maxes out at our frequency of interest ($f = 440\,\mathrm{MHz}$).

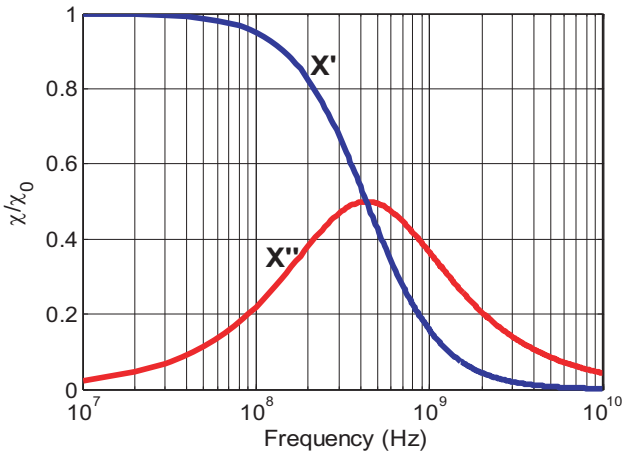

Figure 3. Real and imaginary components of relative susceptibility in the UHF frequency range.

In literature, there is very limited availability of the complex magnetic susceptibility/permeability characterization for magnetite suspensions in the frequency range of interest — with very few available references: permeability measurements for magnetite suspensions in the 0.2–5 GHz frequency range are available in [39]; the impact of particle concentration upon SAR_H was analyzed, for H-field frequencies in the 0.16 GHz range, the critical frequency of these particles (f_c) being empirically estimated for the 1.6–2 GHz range [40]; [41] investigates the influence of the size of the nanoparticles in powder upon the magnetic permeability of magnetite samples at frequencies no higher than 500 MHz. However, the available data clearly demonstrate that there is a need to electrically and magnetically characterize, in the UHF frequency range, tissues with magnetite content, if a realistic assessment of their SAR values is expected; furthermore, for particles with a diameter above 13 nm, the hysteresis loss mechanism is no longer insignificant and should be (separately) assessed. The variation of the coercitive field strength with the radius of the particle (r; in nm) is:

$$H_{coerc}(r) = 200\left(1 - \sqrt{\frac{13}{r}}\right) \tag{18}$$

The authors performed actual field measurements of a portable transceiver emitting at $f = 440\,\mathrm{MHz}$ with an input power of 4 W, which yielded magnitudes of the field strengths of $E = 69\,\mathrm{V/m}$ and $H = 0.35\,\mathrm{A/m}$, at a distance $d = 10\,\mathrm{cm}$ from the antenna in air. For these values, in the (extreme) case where the specific magnetic and electric power dissipations would be equal, $p_m = p_e$, the brain containing magnetite would fulfill the material condition deduced from relation (16):

$$\frac{\varepsilon_r''}{\mu_r''} = 0.37 \tag{19}$$

Should this ratio exceed 0.37, the magnetic dissipation would exceed the electric power dissipation in the brain. Therefore, obtaining information on the actual values of the imaginary parts of the

electric permittivity and magnetic permeability at every frequency is vital, in order to be able to assess the impact of the magnetic dissipation in comparison to the electric dissipation. This is certainly a worthwhile venue for future research.

In the case of the human brain, where a realistic estimation of the magnetite's volumic fraction is $\phi = 3.4 \cdot 10^{-5}$, a $\mathrm{SAR}_H = 1\,\mathrm{W/kg}$ would be obtained if the temperature increment in time would be $\frac{dT}{dt} = 2.7 \cdot 10^{-4\circ}\,\mathrm{C/s}$ (from Eq. (13) using $c_{eff} = 3630.92\,\mathrm{J/kg \cdot K}$). So, a temperature increase of $\Delta T = 0.5°\mathrm{C}$ would be achieved after exposure for $\Delta t = 1.8 \cdot 10^3\,\mathrm{s}$, 30.2 min. On the other hand, had we expected such a SAR to originate from the magnetic component heating alone, as described by the SAR_{H_high} formula, the resulting ratio expected between DC susceptibility and hydrodynamic volume of the particles would be $\frac{\chi_0}{V_H} = 1.6 \cdot 10^{28}$, 10 orders of magnitude greater than the presently known ratio.

3.2. Simulation of the Response of Magnetite-Sprinkled Brain Model to the UHF Wave

The distribution of incident field strengths over vertical planes tangent to the ellipsoidal model of the brain (in air) is presented in Fig. 4; the ground plane and monopole antenna are also visible. The magnitude of the E-field strength in air varies between 20 and 86 V/m in the vertical plane parallel to the antenna, 8 cm from it. In the same plane, the magnitude of the H-field strength varies between 0.15 and 0.56 A/m. The maximum admitted levels for the safe use of emitting devices at the frequency of 440 MHz, as described in electromagnetic field guidelines [1], are set in far-field conditions as $E\_limit = 63\,\mathrm{V/m}$ and $H\_limit = 0.17\,\mathrm{A/m}$. With the observed incident E- and H-fields, the volume loss density distributions in the dielectric brain (no magnetite spheres inserted) case and in the magnetic brain case (five magnetite spheres inserted) are compared in Fig. 5. The left image of Fig. 5 shows the dielectric brain case (the spheres' locations are observable just for reference), and the pure electric volume loss density can be observed; in the right side of Fig. 5, the magnetic brain case is presented, with the total volume loss density mapped (electric and magnetic). The vertical brain section plane contains the centers of three out of the five magnetite spheres; it can be noticed that the volume loss density is highly intensified at the periphery of the magnetite spheres, adjacent to the surface separating

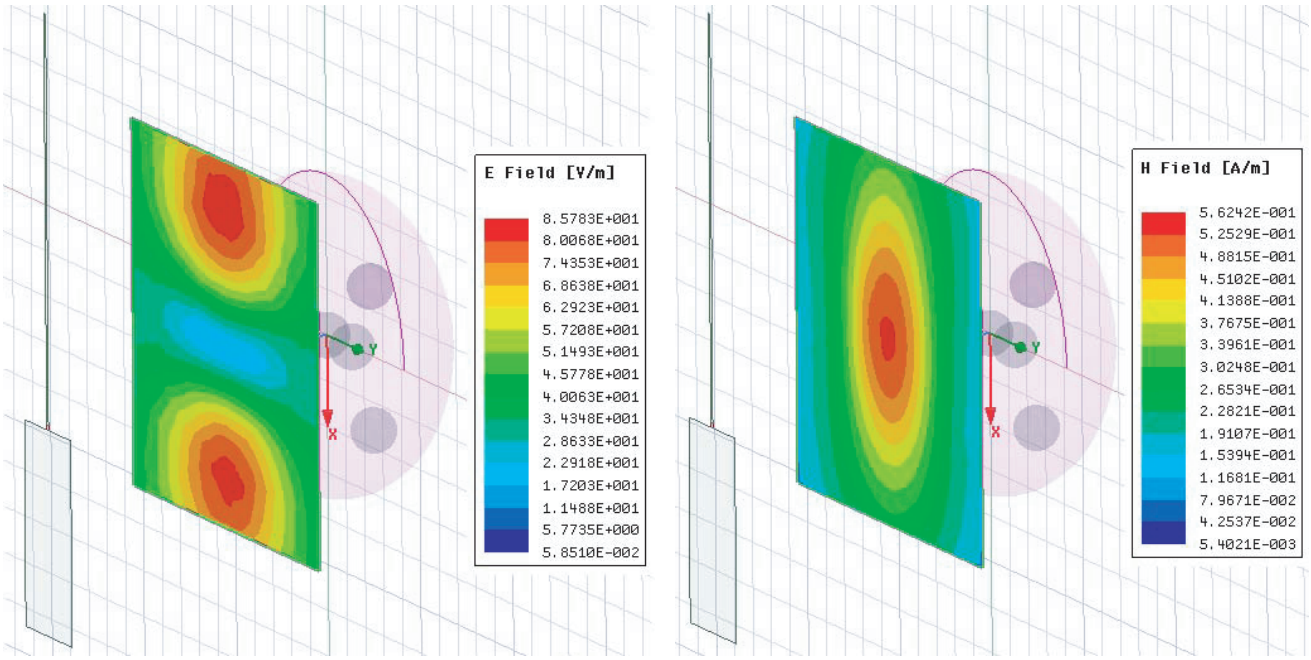

(a) (b)

Figure 4. Map of magnitudes of (a) electric and (b) magnetic near-field components at incidence to the brain model, in air: monopole antenna, $f = 440\,\mathrm{MHz}$, $d = 8\,\mathrm{cm}$ from the source.

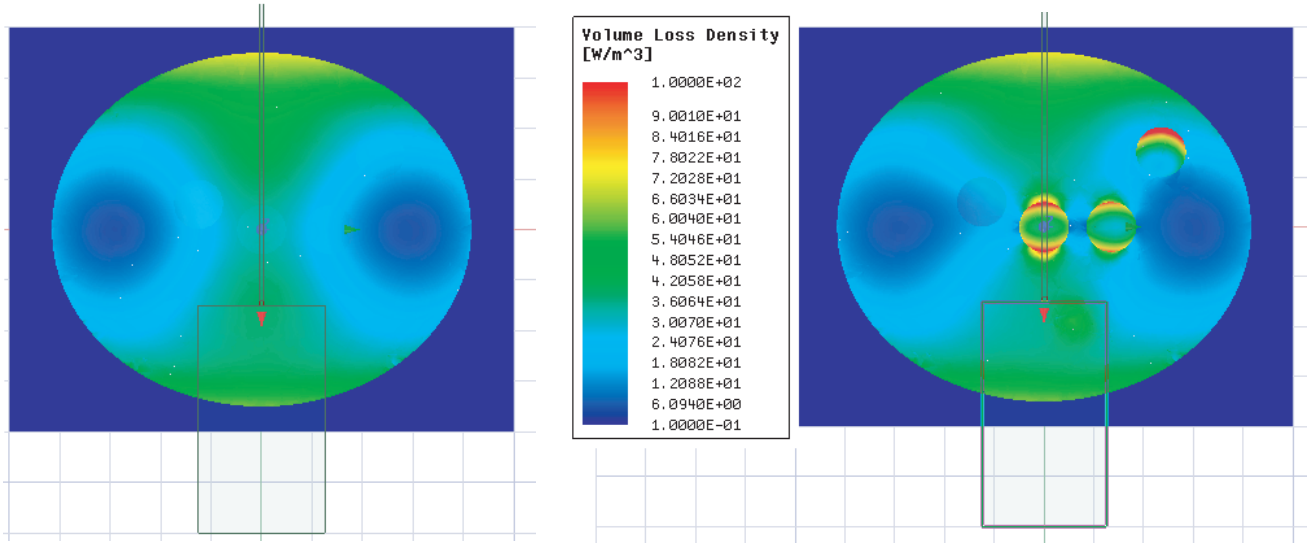

(a) (b)

Figure 5. Maps of volume loss density distribution in a vertical plane sectioning the brain in its center. (a) The "dielectric brain" case — no magnetite present (the sphere locations is observable just for reference). (b) The "magnetic brain" with a volumic fraction of 1.85% magnetite.

them from the environmental tissue. Therefore, the presence of ferrimagnetic material in the dielectric brain changes both the spatial distribution of total power losses (electric and magnetic) and their mean values. The significant increase in losses along the spheres' borders to the surrounding tissue might be a highly important phenomenon and should be carefully followed up separately once magnetic tissues are dosimetrically analyzed.

The total rate of energy deposition in the dielectric brain was computed as SAR = 0.05378 W/kg, whereas the magnetic brain yielded a SAR = 0.05544 W/kg; thus, five magnetite spheres produced a relative increase of the total SAR of 3.1%, corresponding to a volumic fraction of magnetite of $\Phi = 1.85\%$. Yet, as Fig. 5 clearly shows, local power losses at the surface of some of the magnetite particles can be 2–3 times higher than the average losses in the vicinity; this leaves room for noteworthy biological consequences. In particular, we have computed the peak SAR value at the periphery of each of the five magnetite spheres (adjacent to the separation surface with the neighboring cerebral tissue) and noticed that the largest peak SAR was encountered at the surface of sphere 4 — which is situated nearest to the antenna. Its peak SAR was 0.18692 W/kg, which is 3.37 times higher than average SAR in the "magnetic brain". These findings give a clear negative answer to the question whether the presence of magnetite spheres makes brain significantly susceptible to magnetic heating at least in this particular configuration of exposure.

In order to identify how separate components of E- and H-field inside the brain are affected by the presence of magnetite spheres in the organ, we represented the vector field distribution in the same vertical section plane which traverses the center of the brain and the center of three out of the five magnetite spheres. Fig. 6 depicts the E-field vector distribution, comparatively between the dielectric brain (left image) and magnetic brain (right image); it is clearly visible how the three spheres crossed by the sectioning plane cause the modification of vector E's distribution; this fact clearly implies that SAR_H is not simply added to the total SAR when magnetite is present, but also that the SAR_E component changes in response to modifications to the E-field distribution induced by the magnetite present in the tissue. In Fig. 7 the H-field vector distribution is observed comparatively in the same section plane. In the central part of the right image, the change in H vectors' orientation, caused by the presence of magnetite spheres, is clearly visible.

There are a series of limitations in the precise assessment or in the simulation of the dosimetric impact of the presence of even trace amount of ferrimagnetic nanoparticles in dielectric tissues. In the

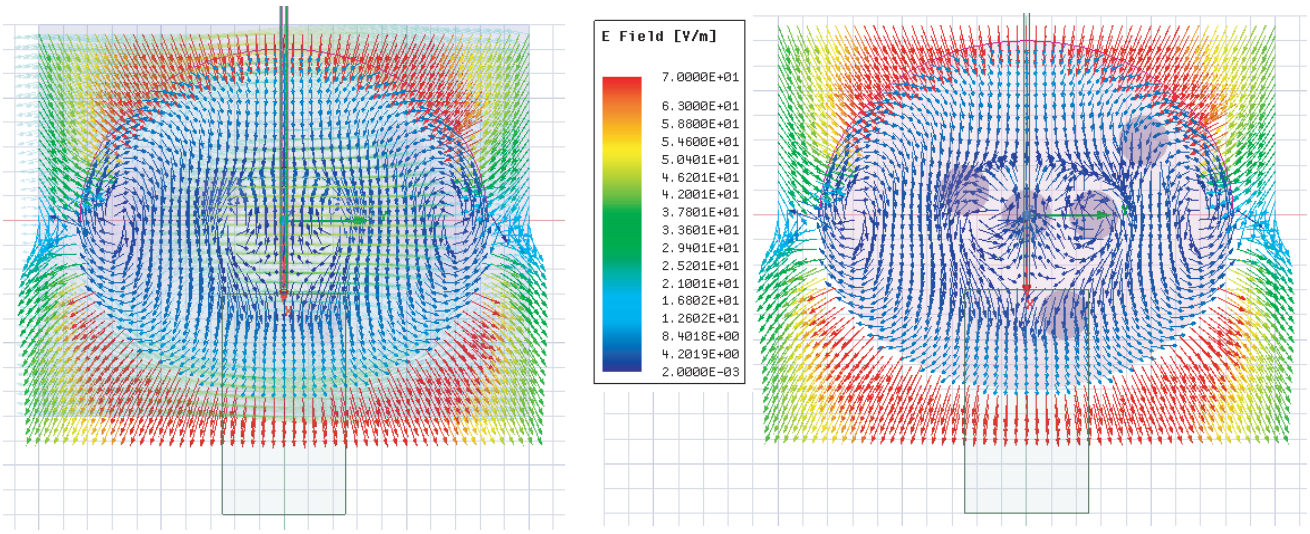

(a) (b)

Figure 6. Maps of vectors of E-field in the brain, in the vertical section plane: (a) "dielectric brain" versus (b) "magnetic brain".

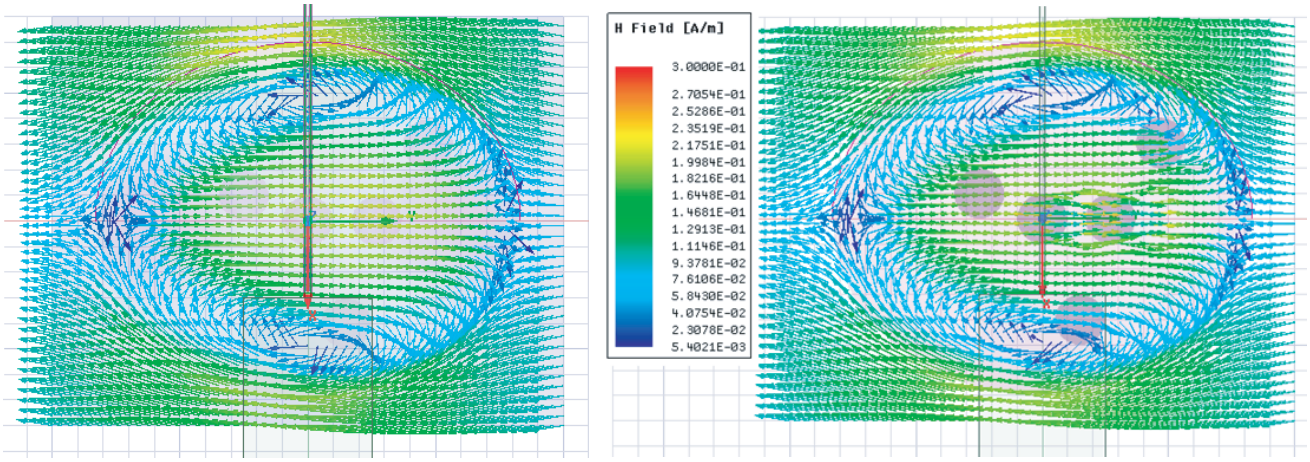

(a) (b)

Figure 7. Maps of vectors of H-field in the brain, in the vertical section plane: (a) "dielectric brain" versus (b) "magnetic brain".

case of brain, we expect that the most important limitation is because the simulations could not take into account the anisotropy of magnetite crystals, which in the hyperthermia studies was shown to have great impact on thermal response. While in hyperthermia, solutions look for to obtain the highest SAR in the nanoparticles volume — and this means to produce them with the desired features (size, shape, crystalline anisotropy, magnetic anisotropy, morphology, degree of aggregation/agglomeration of the nanoparticles). In electromagnetic field exposure of natural tissues, a careful study of properties of the magnetite nanoparticles present in the brain may bring significant and new knowledge about the field interaction with living matter. As long as the magnetite crystals' role in the brain is still unknown, neglecting their presence in the case when significant H-field component in the VHF and UHF ranges is incident on a tissue may be hazardous.

4. CONCLUSIONS

Certain communication devices used in the close proximity of a human head produce significant levels of incident electric and magnetic field components in the UHF range. This study emphasizes the role that magnetite particles found in the human brain, despite their small amount, could have with respect to the power deposition into a tissue which cannot be considered purely dielectric, deposition partially caused by the absorption of the magnetic field component.

The order of magnitude of magnetic power dissipation over the total power loss was estimated using a simple analytical calculation in the context of a continuous wave of frequency $f = 440\,\mathrm{MHz}$ incident on suspensions of magnetite nanoparticles in water. We assumed realistic values for the field strength in air at 10 cm distance from a 4 W portable transceiver: a magnetic field amplitude of 0.35 A/m and an electric field amplitude of 69 V/m. In the case of magnetite nanoparticles uniformly distributed in water at a volumic fraction of $3.4 \cdot 10^{-5}$, with a radius of 6.5 nm, the SAR_H contribution was calculated as $2 \cdot 10^{-6}\,\mathrm{W/kg}$; in this case, the hysteresis loss was ignored, thus only the relaxation processes producing heat were considered. For larger nanoparticles (tens of nm), the relaxation contribution is smaller, $\mathrm{SAR}_H = 10^{-7}$–$10^{-8}\,\mathrm{W/kg}$; for particle diameters larger than 13 nm, it is expected that SAR_H would be higher, due to a significant contribution of hysteresis losses. Equal quantities of specific magnetic and electric power dissipations would be obtained if the ratio between the imaginary parts of permittivity and permeability was 0.37; higher values of this ratio would result in the magnetic dissipation exceeding the electric one. In lack of precise information concerning the complex values of electric permittivity and magnetic permeability for magnetite nanocrystals in the UHF range, it is not possible to estimate the prevalent type of power loss. Therefore, efforts to perform such characterization need to be undertaken.

A comparison of the losses caused by the dielectric properties alone and, respectively, both by the dielectric and the magnetic properties, in a simulation model of the human brain tissue, resulted in a relative increase of total SAR by 3.1% when the magnetic field absorption was taken into account; this increase was achieved with a volumic fraction of magnetite of $1.85 \cdot 10^{-2}$, using magnetite spheres with a 1 cm radius, placed in a realistic volume of homogeneous brain. More significant than the absolute contribution to heat dissipation of magnetite was the discovery of superficial hot-spots, in which the local power losses on the surface of the magnetite particles could be as much as 3.3 times higher than the average losses in the vicinity. It is expected that significant biological consequences are likely to appear, depending on the location and distribution of magnetite crystals in the neurological tissue.

More research is required in order to determine whether the human brain is able to sense and react to specific effects caused by an UHF magnetic field via magnetite nanoparticles. First, for any progress to be possible, a characterization of electric and magnetic properties of biogenic magnetite is necessary in a wide frequency range over UHF band; this would allow obtaining more precise analytical dosimetric results. Second, it is necessary that models of field propagation in much smaller ferrimagnetic particles dispersed in biological dielectrics could be accurately simulated, with a possibility of varying their geometric and magnetic anisotropy constants (which would however need significant computational power). The third research venue is the study of much simpler biological media — such as magnetotactic bacteria suspensions; a combination of experimental dosimetry and physical behavior analysis could enable measurements of not just power losses but potentially highlight non-thermal effects, appearing as forces or torques. The great similarity between biogenic magnetite in the brain and the magnetosomes produced by magnetotactic bacteria represents a noteworthy opportunity for the work in the field.

REFERENCES

1. International Commission on Non-Ionizing Radiation Protection (ICNIRP), "Guidelines for limiting exposure to time varying electric, magnetic, and electromagnetic fields," *Health Physics*, Vol. 74, 494–522, 1998.
2. Rubtsova, N., S. Perov, O. Belaya, et al., "Near-field radiofrequency electromagnetic exposure assessment," *Electromagnetic Biology and Medicine*, Vol. 34, No. 3, 180–182, 2015.
3. Maher, B. A., I. A. M. Ahmed, V. Karloukovski, et al., "Magnetite pollution nanoparticles in the human brain," *Proc. Natl. Acad. Sci. USA*, Vol. 113, No. 39, 10797–10801, 2016.

4. Kirschvink, J. L., A. Kobayashi-Kirschvink, and B. J. Woodford, "Magnetite biomineralization in the human brain," *Proc. Natl. Acad. Sci. USA*, Vol. 89, No. 16, 7683–7687, 2009.
5. Kirschvink, J. L., "Microwave absorption by magnetite: A possible mechanism for coupling nonthermal levels of radiation to biological systems," *Bioelectromagnetics*, Vol. 17, no. 3, 187–194, 1996.
6. Strbak, O., P. Kopcansky, and I. Frollo, "Biogenic magnetite in humans and new magnetic resonance hazard questions," *Meas. Sci. Rev.*, Vol. 11, No. 3, 85–91, 2011.
7. Ueno, S., "Studies on magnetism and bioelectromagnetics for 45 years: From magnetic analog memory to human brain stimulation and imaging," *Bioelectromagnetics*, Vol. 33, 3–22, 2012.
8. Chen, L., C. Chen, P. Wang, et al., "Mechanisms of cellular effects directly induced by magnetic nanoparticles under magnetic fields," *Hindawi. J. Nanomat.*, Vol. 2017, ID 1564634, 2017.
9. Binhi, V. N. and F. S. Prato, "A physical mechanism of magnetoreception: Extension and analysis," *Bioelectromagnetics*, Vol. 38, 41–52, 2017.
10. Hergt, R., S. Dutz, R. Muller, et al., "Magnetic particle hyperthermia: Nanoparticle magnetism and materials development for cancer therapy," *J. Phys.: Cond. Matt.*, Vol. 18, S2919–S2934, 2006.
11. Blaney, L., "Magnetite (Fe_3O_4): Properties, synthesis, and applications," *Lehigh Review*, Preserve 15, paper 5, Lehigh University, 2007.
12. Strbak, O., P. Kopcansky, M. Timko, et al., "Single biogenic magnetite nanoparticle physical characteristics — A biological impact study (for MagMeet 2012 participants)," *IEEE Trans. Mag.*, Vol. 49, 457-462, 2013.
13. Giere, R., "Magnetite in the human body: Biogenic vs. anthropogenic," *Proc. Natl. Acad. Sci. USA*, Vol. 113, No. 43, 11986–11987, 2016.
14. Gorobets, O., S. Gorobets, and M. Koralewski, "Physiological origin of biogenic magnetic nanoparticles in health and disease: From bacteria to humans," *Int. J. Nanomed.*, Vol. 12, 4371–4395, 2017.
15. Cespedes, O. and S. Ueno, "Effects of radio frequency magnetic fields on iron release from cage proteins," *Bioelectromagnetics*, Vol. 30, 336–342, 2009.
16. Carrubba, S., C. Frilot, A. L. Chesson, Jr., et al., "Evidence of a nonlinear human magnetic sense," *Neurosci.*, Vol. 144, 356–367 2007.
17. Carrubba, S., C. Frilot, A. L. Chesson, Jr., et al., "Numerical analysis of recurrence plots to detect effect of environmental-strength magnetic fields on human brain electrical activity," *Med. Eng. Phys.*, Vol. 32, No. 8, 898–907, 2010.
18. Hinrikus, H., M. Bachmann, J. Laas, et al., "Effect of 7, 14 and 21 Hz modulated 450 MHz microwave radiation on human electroencephalographic rhythms," *Int. J. Rad. Biol.*, Vol. 84, No. 1, 69–79, 2008.
19. Suhhova, A., M. Bachmann, D. Karai, et al., "Effect of microwave radiation on human EEG at two different levels of exposure," *Bioelectromagnetics*, Vol. 34, 264–274, 2013.
20. Hinrikus, H., M. Bachmann, D. Karai, et al., "Mechanism of low-level microwave radiation effect on nervous system," *Electromag. Biol. Med.*, Vol. 36, No. 2, 202–212, 2017.
21. Miclaus, S., M. Racuciu, and P. Bechet, "H-field contribution to the electromagnetic energy deposition in tissues similar to the brain but containing ferrimagnetic particles, during use of face-held radio transceivers," *Progress In Electromagnetics Research B*, Vol. 73, 49–60, 2017.
22. Schmid, M. R., M. Murbach, C. Lustenberger, et al., "Sleep EEG alterations: Effects of pulsed magnetic fields versus pulse-modulated radio frequency electromagnetic fields," *J. Sleep. Res.*, Vol. 21, No. 6, 620–629, 2012.
23. Busquets, M. A., A. Espargaró, R. Sabaté, et al., "Magnetic nanoparticles cross the blood-brain barrier: When physics rises to a challenge," *Nanomat.*, Vol. 5, 2231–2248, 2015.
24. Nittby, H., A. Brun, S. Strömblad, et al., "Nonthermal GSM RF and ELF EMF effects upon rat BBB permeability," *Environmentalist*, Vol. 31, No. 2, 140–148, 2011.
25. Salford, L. G., H. Nittby, and B. R. R. Persson, "Effects of electromagnetic fields from wireless communication upon the blood-brain barrier," Sage, C. and Carpenter, D. O. (eds.),

Bioinitiative 2012: A Rationale for Biologically-Based Exposure Standards for Low-Intensity Electromagnetic Radiation (Section 10), Available from: http://www.bioinitiative.org/ report/wp-content/uploads/pdfs/sec10_2012_Effects_Electromagnetic_Fields_Wireless_Communication.pdf, 2012.

26. Deatsch, E. A. and B. A. Evans, "Heating efficiency in magnetic nanoparticle hyperthermia," *J. Mag. Mag. Mat.*, Vol. 354, 163–172, 2014.
27. Ma, M., Y. Wu, J. Zhou, et al., "Size dependence of specific power absorption of Fe_3O_4 particles in AC magnetic field," *J. Mag. Mag. Mat.*, Vol. 268, 33–39, 2004.
28. Jazirehpour, M. and S. A. Seyyed Ebrahimi, "Effect of aspect ratio on dielectric, magnetic, percolative and microwave absorption properties of magnetite nanoparticles," *J. Alloys Comp.*, Vol. 638, 188–196, 2015.
29. Khurshid, H., J. Alonso, Z. Nemati, et al., "Anisotropy effects in magnetic hyperthermia: A comparison between spherical and cubic exchange-coupled FeO/Fe_3O_4 nanoparticles," *J. Appl. Phys.*, Vol. 117, 17A337, 2015.
30. Vasilakaki, M., C. Binns, and K. N. Trohidou, "Susceptibility losses in heating of magnetic core/shell nanoparticles for hyperthermia: A Monte Carlo study of shape and size effects," *Nanoscale*, Vol. 7, No. 17, 7753–7762, 2015.
31. Shubitidze, F., K. Kekalo, R. Stigliano, et al., "Magnetic nanoparticles with high specific absorption rate of electromagnetic energy at low field strength for hyperthermia therapy," *J. Appl. Phys.*, Vol. 117, No. 9, 094302, 2015.
32. Jazirehpour, M. and S. A. Seyyed Ebrahimi, "Synthesis of magnetite nanostructures with complex morphologies and effect of these morphologies on magnetic and electromagnetic properties," *Ceramics Int.*, Vol. 42, 16512–16520, 2016.
33. Liu, X., K. Cao, Y. Chen, et al., "Shape-dependent magnetic and microwave absorption properties of iron oxide nanocrystals," *Mat. Chem. Phys.*, Vol. 192, 339–348, 2017.
34. Dolník, B., M. Rajnák, R. Cimbala, et al., "The response of a magnetic fluid to radio frequency electromagnetic field," *Acta Phys. Pol. A*, Vol. 131, No. 4, 946–948, 2017.
35. Marin, C. N., I. Malaescu, and P. C. Fannin, "Theoretical evaluation of the heating rate of ferrofluids," *J. Therm. Anal. Calorim.*, Vol. 119, No. 2, 1199–1203, 2014.
36. Attar, M. M. and M. Haghpanahi, "Effect of heat dissipation of superparamagnetic nanoparticles in alternating magnetic field on three human cancer cell lines in magnetic fluid hyperthermia," *Electromag. Biol. Medicine*, Vol. 35, No. 4, 305–320, 2016.
37. Skumiel, A., M. Kaczmarek-Klinowska, M. Timko, et al., "Evaluation of power heat losses in multidomain iron particles under the influence of ac magnetic field in RF range," *Int. J. Thermophys.*, Vol. 34, 655–666, 2013.
38. Fannin, P. C., I. Malaescu, C. N. Marin, et al., "Microwave specific loss power of magnetic fluids subjected to a static magnetic field," *Eur. Phys. J. E*, Vol. 27, 145–148, 2008.
39. Fannin, P. C., I. Malaescu, C. N. Marin, et al., "Microwave propagation parameters in magnetic fluids," *Eur. Phys. J. E*, Vol. 29, 299–303, 2009.
40. Malaescu, I., C. N. Marin, M. Bunoiu, et al., "The effect of particle concentration on the heating rate of ferrofluids for magnetic hyperthermia," *Annals of West University of Timisoara — Physics*, Vol. 58, No. 1, 81–88, 2015.
41. Yun, H., X. Liu, T. Paik, et al., "Size- and composition dependent radio frequency magnetic permeability of iron oxide nanocrystals," *American Chem. Soc. Nano*, Vol. 8, No. 12, 12323–12337, 2014.